Article

Multichannel real-time electronics platform for the estimation of the error in impact localization with different piezoelectric sensors density

Lorenzo Capineri [1,] *, Andrea Bulletti [2] and Eugenio Marino Merlo [3]

[1] Department of Information Engineering, University of Florence; lorenzo.capineri@unifi.it
[2] Department of Information Engineering, University of Florence; andrea.bulletti@unifi.it
[3] Department of Information Engineering, University of Florence; eugenio.marinomerlo@unifi.it
* Correspondence: lorenzo.capineri@unifi.it

† This paper is an extended version of our paper published in A. Bulletti, E. M. Merlo and L. Capineri, "Analysis of the accuracy in impact localization using piezoelectric sensors for Structural Health Monitoring with multichannel real-time electronics," 2020 IEEE 7th International Workshop on Metrology for AeroSpace (MetroAeroSpace), Pisa, Italy, 2020.

Abstract: The work presents a Structural Health Monitoring (SHM) electronic system with real-time acquisition and processing for the determination of impact location in laminate. The novelty of this work is the quantitative evaluation of impact location errors using the Lamb wave guided mode S_0, captured and processed in real-time by up to eight piezoelectric sensors. The differential time of arrival is used to minimize an error function for the position estimation. The impact energy is correlated to the amplitudes of the antisymmetric (A_0) mode and the electronic design is described to avoid saturation for signal acquisition. The same electronic is designed to acquire symmetric (S_0) low level signals by adequate gain, bandwidth and signal to noise ratio. Such signals propagate into a 1.4mm thick aluminum laminate at the group velocity of 5150m/s with frequency components above 270kHz and can be discriminated from the A_0 mode to calculate accurately the differential arrival time. The results show that the localization error stabilizes at a value comparable with the wavelength of the S0 mode by increasing the number of sensors up to six, and then remaining constant up to eight sensors. This suggests that a compromise can be found between sensor density and localization error.

Keywords: real-time electronics, structural health monitoring, Lamb wave, piezoelectric sensors, impact localization, ultrasonic guided waves

1. Introduction

The Structural Health Monitoring (SHM) has been subject to different studies in the Non-destructive testing (NDT) field also aimed to the identification of the location of the impact point using piezoelectric sensors. Many plate-like geometries made in fiber-reinforced composite (CFRP) or aluminum commonly used in aerospace structures, are suitable to support the guided propagation of ultrasound guided waves over long distance; for plate like structures few mm thick we refer to extensional and flexural modes of Lamb waves. The possibility of identifying damage on a structure by piezoelectric sensor systems allows for the determination of its integrity, thus reducing downtime and maintenance costs. SHM is important because by continuous monitoring, it permits real-time detection of damage in a structure, particularly of safety-critical components typical of the application of compounds in the aircrafts [1–5]. A real-time SHM system with a passive sensors networks, is proposed to detect low and high impact events. For each event, the conversion of kinetic energy into propagating ultrasonic guided waves occurred and the acoustic emission (AE) localization methods can be applied by using piezoelectric transducers. Once a localization is performed, the SHM system can be switched to the active

 doi:10.20944/preprints202104.0595.v1

mode operation to investigate a restricted the area around the estimated impact position. Array of sensors and real time multichannel electronic processing are the enabling technology for the applications of SHM in aerospace, energy conversion, transportation, and automotive industry.

In the literature different strategies for locating impact positions using Lamb waves are investigated with reference to the extraction of the Differential Time of Arrival (DToA). Tobias in [6] uses a triangulation technique; Ciampa and Meo in [7] evaluate the DToA with an algorithm based on Continuous Wavelet Transform (CWT); Shukri Mohd et al. in [8] use a method based on Wavelet Transform Analysis and Modal Location (WTML) with four sensors; Shenxin Yin et al. in [9] work on using eight sensors bonded in a "Z" shaped arrangement. While the CWT allows more sophisticated signal processing for the separation of the flexural and extensional dispersive modes, in a multisensory system with several nodes it must be considered also the simpler solution like the first arrival signal detection with threshold method or short time Fourier Transform (STFT). The latter, requires less computational resources than CWT but it does not permit the trade-off between the arrival time and spectral content.

For complex three-dimensional structures the analysis of the DTOA relative to propagation along multiple paths is not straightforward and difficult to treat with analytical models. In these cases are often used multiple sensors and artificial intelligence (AI); for example the system based on neural networks presented by Worden et al. [10] use up to 17 sensors. Carrino et al. [11-12] proposed an innovative method based on nonlinear Lamb waves for locating disbonds in single-lap joints that uses PZT signals processed with a baseline-free algorithm and the localization of artificial defects placed inside the area delimited by four PZT sensors.

Other strategies for locating impact positions also without knowing the characteristics of the material under test are reported in [13-14]. In a previous work Kundu et al. [14], presented a study that considers different shapes of the wave front generated during an acoustic event and develops a methodology to localize the acoustic source in an anisotropic plate from those wave front shapes: an elliptical wave front shape-based technique was developed first, followed by the development of a parametric curve-based technique for non-elliptical wave front shapes. This methodology does not assume a straight-line wave propagation path and can predict the source location without any knowledge of the elastic properties of the material; however, this study reports only a theoretical approach without developing a real-time system to validate the proposed technique.

In [15], the authors of this work presented a guided-wave ultrasound SHM system based on linear arrays of interdigital piezopolymer transducers bonded to a composite pressure vessel for spacecraft. In that system, interdigital transducers were adopted to perform both damage assessment and impact detection/localization using a simple fixed-threshold technique. In a related research development [16], the authors presented a novel approach to estimate the DToA between the impact response signals collected by a triplet of sensors, overcoming the limitations of classical methods that rely on amplitude thresholds calibrated for a specific sensor type. Finally, in [17] is proposed a simple laboratory procedure based on a set-up with a pair of sensors that are symmetrically placed with respect to the impact point, to estimate the uncertainty of the DToA and the propagation velocity.

In this work we have upgraded the real-time electronic system reported in [15] that allows to accommodate the analog front-end electronics characteristics thanks to a modular design; different sensor types (piezoceramic, piezocomposites, piezopolymers) need custom analog front end (AFE) to match the electrical impedance, sensitivity, and bandwidth. In this work we designed and implemented 16 new receiver boards to collect information of the propagated extensional S_0 mode Lamb waves thanks to the improved bandwidth, adjustable gain, and signal to noise ratio. This new feature allows to overcome the limitation of using the information for the localization carried by the higher level but slower A_0 mode. The detection of small amplitude (mV-10 mV) S_0 mode signal with

Preprints (www.preprints.org) | NOT PEER-REVIEWED | Posted: 22 April 2021 doi:10.20944/preprints202104.0595.v1

threshold method simplifies the electronic design with benefits also on power consumption and rapid event detection. As observed in [18] [19], A_0 mode propagates on longer paths with low attenuation but at lower propagation velocity and exhibits dispersion phenomena in the low frequency range. Such characteristics complicate the interpretation of the impact generated signals especially considering large structures and multiple reflections from boundary, then in many cases S_0 is preferred. Moreover, the importance of sensors networks for aircraft SHM was reported in [20] considering the large dimensions and the trade-off between system performance, reliability, and cost.

The study presented in this paper differs from previously cited works because the aim is not to present the best method or technique for locating impact positions but to report the analysis of errors on impact localization (see Section 2) using real-time electronics; the paper present also the evaluation of the influence of the number of passive PZT sensors used (see section 3) on the position error. The real time electronics can also acquire multiple impacts on the same point for statistical analysis. We present the results of experimental tests with low energy impact on a 1.4 mm thick aluminum plate using Physik Instrumente P-876.SP1 piezoceramic transducers, varying the number of channels from four to eight. The signals are then used to find the minimum of a cost function for the localization of the impact and therefore the evaluation of the positioning error relative to the size of the investigation area and the number of passive channels used and the results are reported in Section 4 and discussed in the Conclusions. Finally, to help the reader finding selected topics we include in Appendix A a list of acronyms used in the paper.

2. Impact Detection and Localization

Considering a plate-like structure, a point impact on the surface will determine a mechanical response in the form of elastic waves of various nature propagating outward from the point of contact. Our work was focused on detecting low-energy impacts (from 35mJ to 600mJ) that do not result in permanent damage of the aluminum plate. Low energy impacts are of interest for laboratory testing on system prototypes because are non-destructive, while larger energy (>1J) impacts are used for real-life SHM applications. The implication on the sensor choice regarding the sensitivity and impact energy will be tackled in the next section.

In general, it is possible to detect the location of an impact event by measuring the DToAs of the elastic response wave front to a set of three or more sensors knowing their position (x_i, y_i) on a planar structure. Using these data, the impact location can be numerically triangulated. Our system estimated the DToA of impact-generated elastic waves using a simple amplitude threshold thanks to the remarkable (better than 70 dB) signal to noise ratio (SNR) of the analog front-end.

The developed system performed impact detection by running in passive (listening) mode, i.e., by continuously sampling the transducer signals in a circular buffer, while waiting from a triggering event (a threshold-crossing) to occur. This threshold level (six time the root-mean-square noise level) had to be verified during the experimental tests to avoid spurious triggering, while maintaining a good sensitivity to low-energy impacts. As the data acquisition hardware detected an impact threshold crossing event, it immediately froze the circular buffer and transferred the data to the acquisition system.

We defined a Region of Interest (ROI) of the aluminum plate equal to 250mm x 240mm (see Figure 1) and this area was divided into a uniform grid of points spaced 1 mm with coordinates (x_P, y_P) for the following analysis. For each of those points, the impact localization algorithm processed the received signals to extract the differential DTOAs and calculated the value of the error function $E(x_P, y_P)$ [15-17]. Once the error function (1) was calculated for the whole grid, the impact point was assigned by the absolute minimum error value criterion. The error function $E(x_P, y_P)$ presents a minimum and has a monotonic behavior. In such cases, one can extrapolate a best-guess position of the impact by calculating the centroid of the points having a value within 1% of the absolute minimum.

Preprints (www.preprints.org) | NOT PEER-REVIEWED | Posted: 22 April 2021 doi:10.20944/preprints202104.0595.v1

The choice of grid of points spaced 1 mm was a good compromise between the accuracy of the estimation of the impact point and the necessity to elaborate signals in real-time showing immediately the results on a PC display.

$$E(x_p, y_p) = \sum_{i=1}^{N_T-1} \sum_{j=i+1}^{N_T} \left| \frac{(t_i - t_j)v - \left(\sqrt{(x_i - x_p)^2 + (y_i - y_p)^2} - \sqrt{(x_j - x_p)^2 + (y_j - y_p)^2} \right)}{\sqrt{(x_i - x_j)^2 + (y_i - y_j)^2}} \right| \quad (1)$$

Where N_T is the total number of installed sensors and their positions are defined by the coordinates $P_i=(x_i, y_i)$ and $P_j=(x_j, y_j)$. The corresponding measured time of flights for each sensor are t_i and t_j respectively.

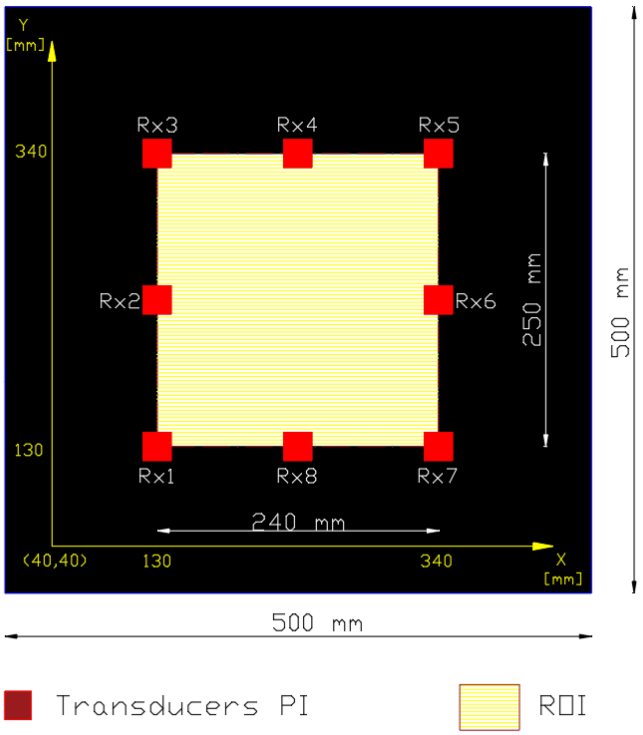

Figure 1. The picture shows the 1.4mm thick aluminum plate with 8 sensors arrangement (red squares). Picture reports also the indication of the ROI (yellow area) and the area outside the ROI (black area) that corresponds to the aluminum laminate dimension.

3. Experimental set-up and electronic equipment

This section describes the electronic system designed for SHM application using multiple sensors in passive mode. The system can also be switched automatically in active mode for damage assessment by using interdigital transducers as reported in [15].

3.1. Electronic instrument design for SHM evaluation

The main architecture design of the electronic instrument developed as part of this work has been presented in [21]. The instrument consists of a 16-channels fully programmable as active or passive mode operations. One of the main characteristics of this electronic system is the real-time acquisition and processing of ultrasonic signals received by 16 channels, that is an advantage for the research of a sensors layout with more than 3 or 4 channels; the latter is a quite common experimental situation being available with a digital oscilloscope.

For the passive operation mode, treated in this work, we designed 16 new receiver boards that easily replaced the previous ones thanks to the modular architecture of the system. A block-scheme of the new board is shown in Figure 2. The input attenuator is a

Preprints (www.preprints.org) | NOT PEER-REVIEWED | Posted: 22 April 2021 doi:10.20944/preprints202104.0595.v1

fundamental block to adjust for different sensor sensitivity and impact energy. For example, impacts with from 10 mJ to 100 mJ energy can be monitored with 6.5 mm PVDF circular type (see [16][17]) producing voltage signals in the range of 100mV to 1V, while the highest sensitivity of piezoceramic sensors like Physik Instrumente P-876.SP1 allows signals up to 300 mVpp with the low energy impact hammer or free-falling sphere, typically used during non-destructive laboratory tests. The piezoceramic material of this type of sensors has a high electromechanical coupling factor and high sensitivity.

The two different type of piezoelectric sensors used are shown in Figure 2 and their signal output amplitude are measured by direct connection to a digital oscilloscope; the comparison of the amplitudes is reported in Figure 3 for different impact energy from 0 to 45 mJ. In Figure 3 we can observe different energy values, U=m×g×h, corresponding to the same value of mass of the impacting steel sphere: these different values are obtained according to relationships by varying the falling height h and gravity acceleration g.

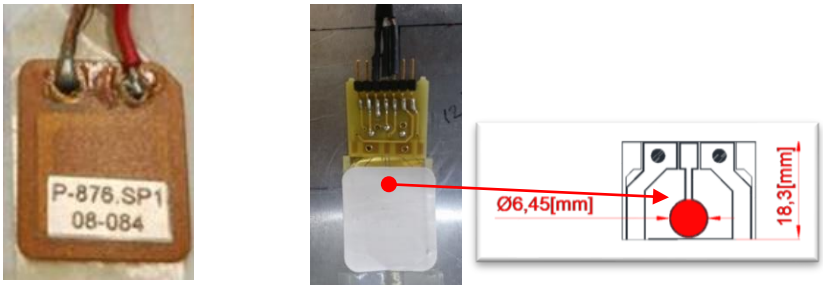

Figure 2 – (Left) Piezoceramic sensor PI_876.SP1. Piezopolymer (PVDF) sensor protected by a white adhesive label and electrical connections on a PCB . (Right) Circular element of 6.45 mm diameter shown by the red circle on the CAD drawing.

These amplitudes are relative to the peak amplitude of the large A_0 mode which is generated by the impact and has low frequency components, typically below 50 kHz as predicted by Ross in [23]. The data reported in Figure 3 are important to decide the programmable threshold value depending on the expected impact energy. In this way the real time electronics captures the signals with a predefined minimum energy and thanks to the programmed pre-trigger time, the signal trace also contains the information of signals preceding the large A_0 mode. This is a relevant feature for the electronics system because higher frequency components of the A_0 and S_0 propagates at higher velocities, as explained later in Section 4 and in Figure 7.

Preprints (www.preprints.org) | NOT PEER-REVIEWED | Posted: 22 April 2021 doi:10.20944/preprints202104.0595.v1

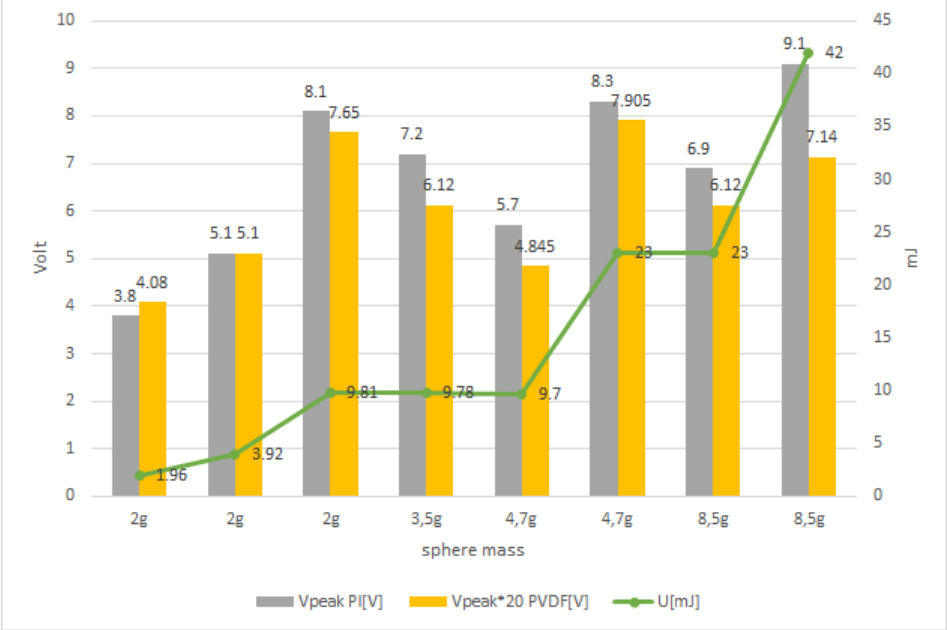

Figure 3 - Peak voltages from impacts generated by steel balls with mass ranging from 2g to 8.5g in free-fall on the aluminum laminate. The sensitivity of the two different sensors (see Figure 2) can be compared by the output voltages: the PVDF sensor amplitudes are multiplied by a constant factor 20 to be compared with the trend of the PZT amplitude. We can observe the good correlation between impact energy and the output voltage.

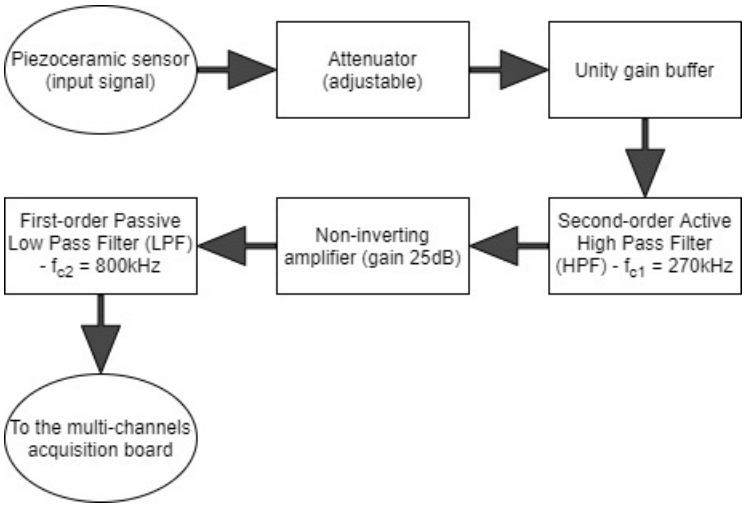

Figure 4. The block-scheme of the new design of the receiver board.

The electronic analog front-end (AFE) (see figure 4) is mainly composed by a programmable input attenuator (from 0 to -20dB), a unity gain buffer based on LF347 op amp, a non-inverting amplifier with voltage gain of 25dB based on a LM6172 op amp and a band pass filter (BPF). The BPF is obtained designed an active (op amp LM6172) second-order Bessel HPF with the cut-off frequency (fc1) equal to 270kHz @ -3dB and a passive first-order LPF with the cut-off frequency (fc2) equal to 800kHz @ -3dB. The last filtering block is inserted to limit the in-band noise; in Table 1 are reported the noise measurements of the output of the analog chain with a standard 50 Ohm input impedance for two different prototype boards.

Preprints (www.preprints.org) | NOT PEER-REVIEWED | Posted: 22 April 2021 doi:10.20944/preprints202104.0595.v1

Table 1: V_{rms} output noise of the front-end channel with input impedance 50 Ω and attenuator selected at 0dB

	$V_{rms}out$ front-end #1	$V_{rms}out$ front-end #2
Zin = 50 Ω	1m V	1m V

These values are adequate considering the low voltage analog to digital converter (ADC) has 12 Bit resolution and input dynamic of 3.3V present on the electronic platform. Moreover, we observe that the programmable attenuator is necessary to limit the input signal in the AFE chain to avoid saturation and to protect the first amplifier from large signal exceeding the allowable common mode range at the operating frequency.

The main difference respect to the previous version [21] is the receiver versatility that can be programmed to receive ultrasonic impact signals that in general include S_0 and A_0 modes. The possibility to receive higher frequencies up to 270 kHz with high signal to noise ratio (10dB) to analyze S_0 Lamb modes that propagate at higher velocities respect to A_0 modes and with lower amplitude.

An example of the output signal after the analog processing stage is shown in Figure 5. The fast S_0 mode and the high frequency component of the A_0 mode are now present in the signal. The early S_0 mode signal will be used later for the calculation of the DTOAs for the impact localization by triangulation algorithm.

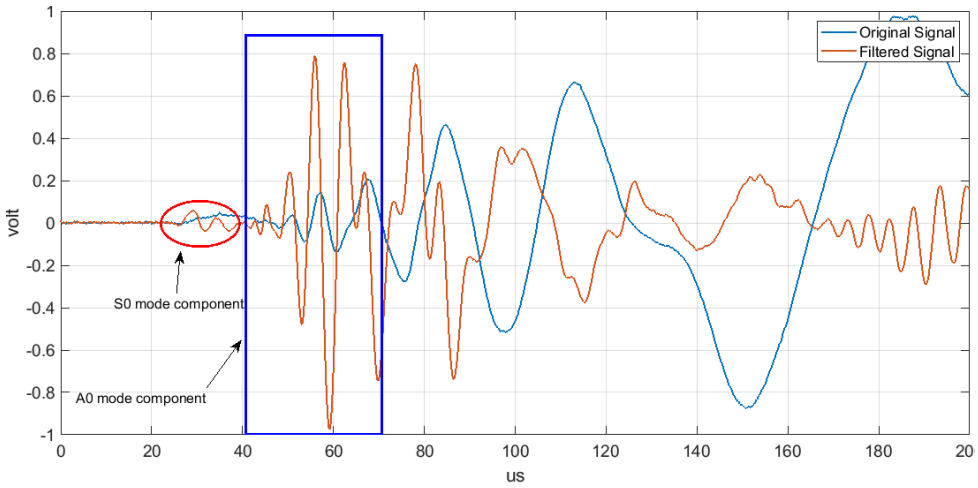

Figure 5: Comparison between original signal and filtered signal with high-pass second order filter, with cut-off frequency 270 kHz followed by a 25 dB gain amplifier (see Figure 4). The signals are normalized, the distance between the impact point and the sensor is 10 cm. The two ultrasonic guided modes A_0 (pointed out in blue) and S_0 (pointed out in red) are well discriminated with high SNR.

3.2. Experimental set-up

In Figure 6 (Right) are described the main blocks and connection of the SHM system.

The main characteristics of the data acquisition system are listed in the following:

Programmable parameters:

- VGA gain from 54dB to 90dB to adjust for different sensors sensitivity,
- High Voltage up to 100V for active mode operation
- Square wave burst (1-16 cycles) up to 500kHz for active mode operation.

Preprints (www.preprints.org) | NOT PEER-REVIEWED | Posted: 22 April 2021 doi:10.20944/preprints202104.0595.v1

Data Acquisition system characteristics:

- 12-bit resolution,
- 16-channels at 20MSps,
- Storage: 1MS per channel

The main components of the block diagram for the data acquisition system are:

(1) Sensor layout installed on the plate-like structure, coordinate reference system, and impact point markers (#1, #2, #3, #4, #5, etc.)

(2) signal conditioning electronics.

(3) multichannel VGA with ADC evaluation module (Texas Instruments AFE5851EVM, Dallas, TX, USA).

(4) Spartan-6 FPGA evaluation card (Xilinx SP605).

The experimental set-up adopted is reported in Figure 6 (left), where only 8 out of 16 channels are programmed for passive monitoring of impacts. Figure 6 (left) shows the low-energy hammer impactor in the center of the aluminum plate where the eight piezoelectric sensor arrangement was placed. The eight sensors have been placed along the perimeter of the ROI (see Figure 1) and their arrangement is shown in the section of experimental results.

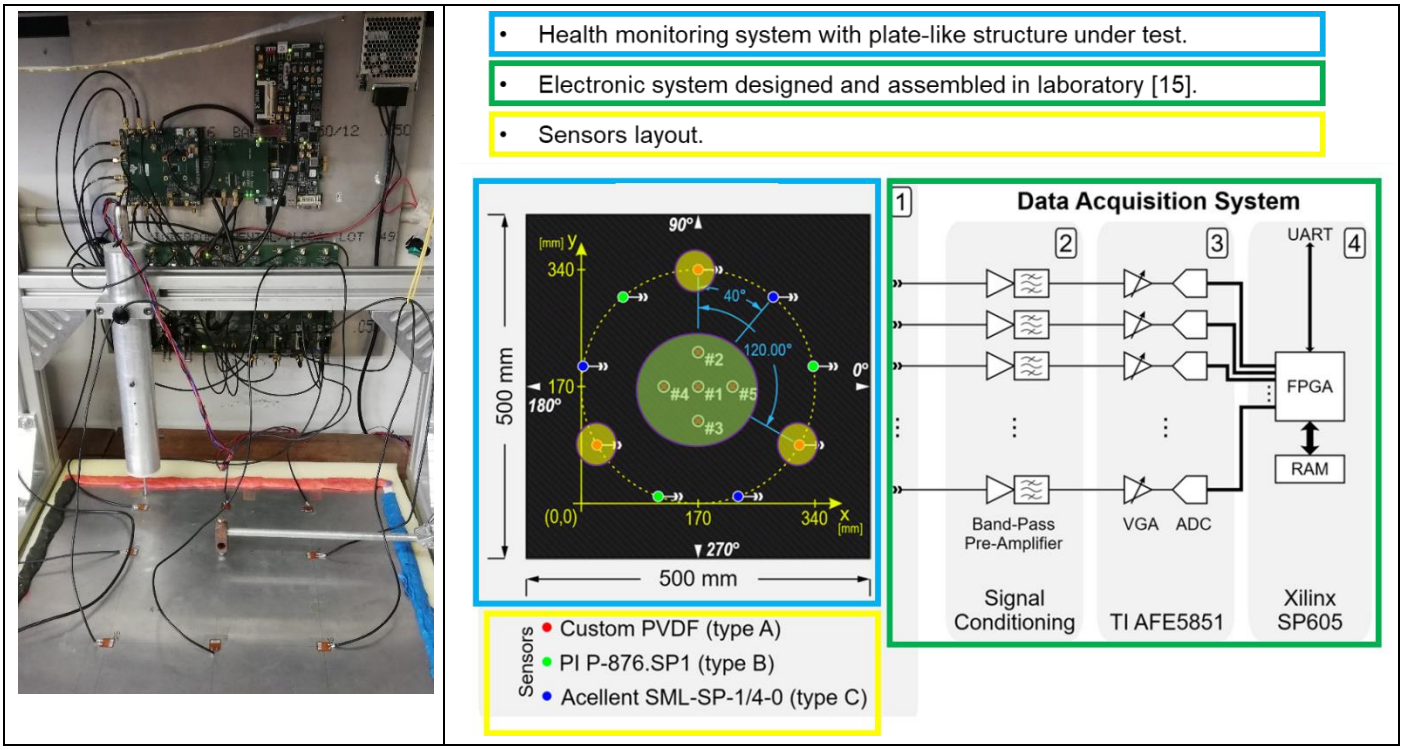

Figure 6. Experimental set-up with the eight piezoceramic transducers attached with a bi-adhesive tape in a 1.4mm aluminum plate shown in the bottom of the figure and the real-time electronic acquisition system shown in the top. In the center of the plate the low-energy hammer impactor is visible. Figure also shows the colored play dough covering the edges of the aluminum plate edges; this method adopted to attenuate the signals received from multipath. Reproduced from [24].

The high number of sensors enable also to reveal impacts outside the ROI up to the full size of the aluminum plate. The four edges of the aluminum plate are covered by colored play dough (see the colored edges in Figure 6) to avoid spurious reflections of the

Preprints (www.preprints.org) | NOT PEER-REVIEWED | Posted: 22 April 2021 doi:10.20944/preprints202104.0595.v1

ultrasonic signal due to the edges. This simple method turned out to be necessary to manage the boundary reflection due to the free edges of plate for estimation of impacts position carried out outside the ROI. The problem concerning the multiple reflections from the plate edges can also be addressed by selecting a time according to the geometry of the plate-like structure [17]. More clever algorithms exploit also the information retrieved by multiple reflections from boundaries for keeping low the number of sensors installed on the structure [22].

Next section reports the analysis of different errors obtained for different impact points (inside and outside the ROI) and for different number of channels used to find the minimum of function (1).

4. Experimental Results

The new custom real-time acquisition system has been tested in a series of low-energy impacts loading experiments to not induce damages into the laminate. The aim of those experiments was to verify the actual capabilities of the SHM system (i.e., the localization accuracy) processing signal acquired from different number of sensors.

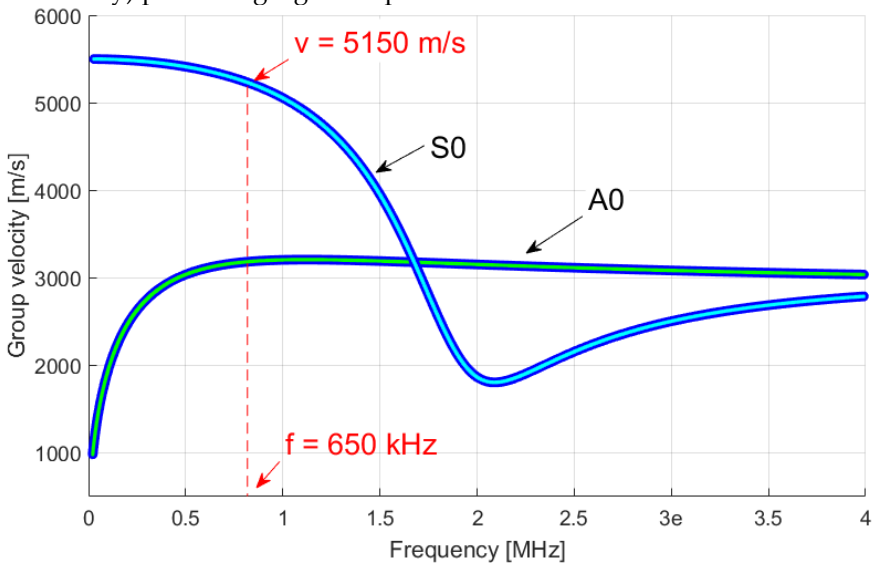

Figure 7. The viewgraph shows the calculated S_0 and A_0 group velocity dispersion curves for an aluminum plate with thickness of 1.4mm.

The fundamental symmetric (S_0) and anti-symmetric (A_0) group velocity dispersion curves for an aluminum plate with thickness of 1.4mm are shown in Figure 7. These curves have been obtained with the LAMB MATLAB® toolbox GMM calculator. From Figure 7 we can evaluate the propagation velocity of the S_0 mode. This value will be used to solve the equation (1). For our experiments we consider the propagation velocity v = 5150m/s corresponding to a frequency of fS0=650kHz which fall into a frequency range where dispersive behavior of S_0 mode is negligible but still retain a small wavelength v/fS0=8 mm.

We performed three impacts: impact P1 with position x_i = 190mm; y_i = 150mm performed inside the ROI delimited by sensors; impact P2 with positions position x_i = 193mm; y_i = 32mm performed outside the ROI and impact P3 with positions position x_i = 200mm; y_i = 40mm performed outside the ROI.

In Figures 8, 9, 10, 11, 12 and 13 we reported the results for impact's position inside and outside the ROI.

In detail, Figure 8 shows performance of the acquisition system detecting impact point P1 processing the signal acquired by only four sensors Rx1, Rx3, Rx5, Rx7 whereas Figure 9 shows the result obtained detecting impact point P1 processing the signal acquired by the all eight sensors (Rx1-Rx8). The estimated position of the impact point obtained by processing signals acquired by only four sensors (P1'-1 point) is also reported

Preprints (www.preprints.org) | NOT PEER-REVIEWED | Posted: 22 April 2021 doi:10.20944/preprints202104.0595.v1

in Figure 8, whereas Figure 6 shows the estimated position of the impact point obtained by processing signals acquired by the all sensors (P1′-2 point). To evaluate the trade-off between sensor density of a SHM system and error in impact localization we process the signal acquired by six sensors Rx1, Rx2, Rx3, Rx5, Rx6, Rx7 and the estimated position of the impact point (P1′-3 point) is reported in Figure 10.

Results shown in Figures 8, 9 and 10 are summarized in Figure 11.

In general, the installation of sensor is based on several constraints imposed by the target structure while the impact event position is more unpredictable. Then is worth to analyze impacts outside the ROI, the full size of the area of the aluminum plate (500mm x 500mm) was divided into a uniform grid of points spaced 1 mm with coordinates (x_P, y_P). Figure 12 and Figure 13 show the result obtained processed signals acquired from all sensors in case of impact P2 and P3 outside the ROI.

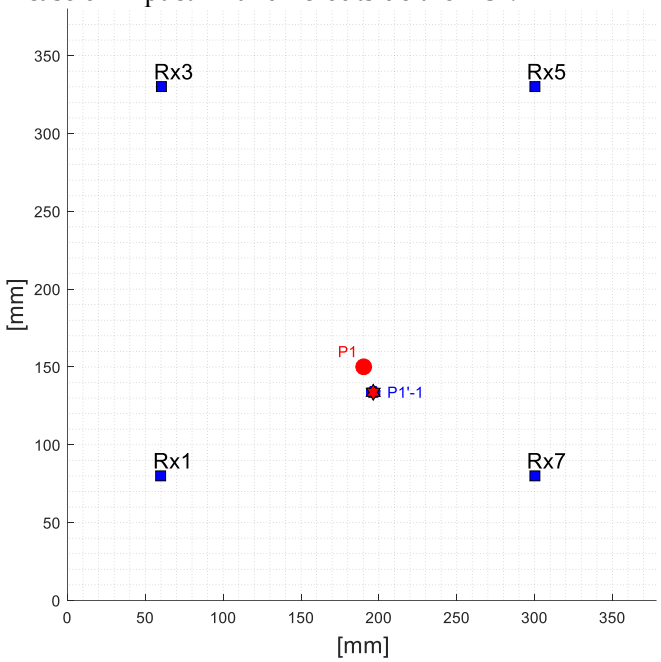

Figure 8. Position of impact P1 (red circle) inside the ROI with coordinates xi = 190mm; yi = 150mm. The detected impact position P1′-1 (red star) with coordinates xp = 196mm; yp = 134mm has been obtained by processing the ultrasonic signals acquired by only four sensors (Rx1, Rx3, Rx5, Rx7). Reproduced from [24].

Preprints (www.preprints.org) | NOT PEER-REVIEWED | Posted: 22 April 2021 doi:10.20944/preprints202104.0595.v1

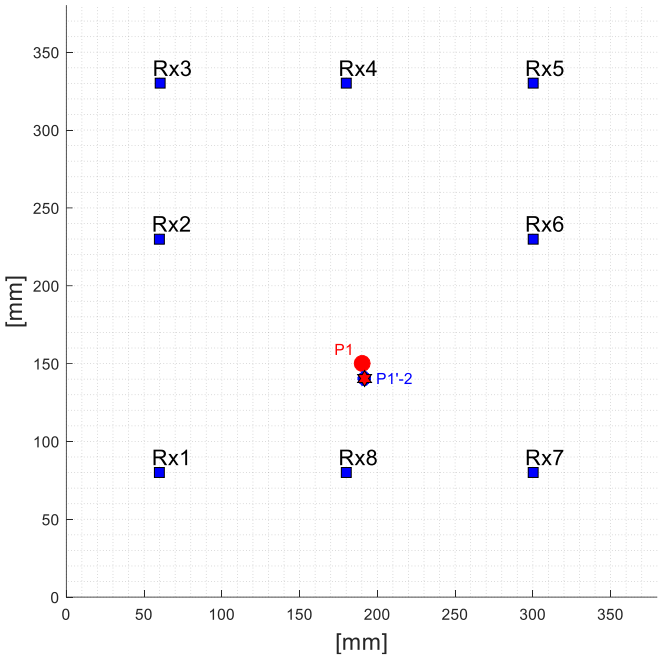

Figure 9. Position of impact P1 (red circle) inside the ROI with coordinates xi = 190mm; yi = 150mm. The detected impact position P1′-2 (red star) with coordinates xp = 192mm; yp = 141mm has been obtained by processing the ultrasonic signals acquired by all sensors (Rx1-Rx8). Reproduced from [24].

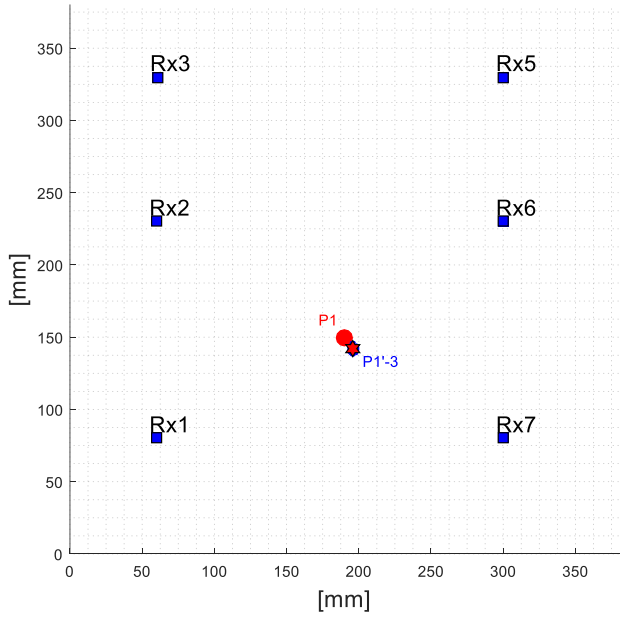

Figure 10. Position of impact P1 (red circle) inside the ROI with coordinates xi = 190mm; yi = 150mm. The detected impact position P1′-3 (red star) with coordinates xp = 196mm; yp = 142mm has been obtained by processing the ultrasonic signals acquired by six sensors (Rx1, Rx2, Rx3, Rx5, Rx6, Rx7).

Preprints (www.preprints.org) | NOT PEER-REVIEWED | Posted: 22 April 2021 doi:10.20944/preprints202104.0595.v1

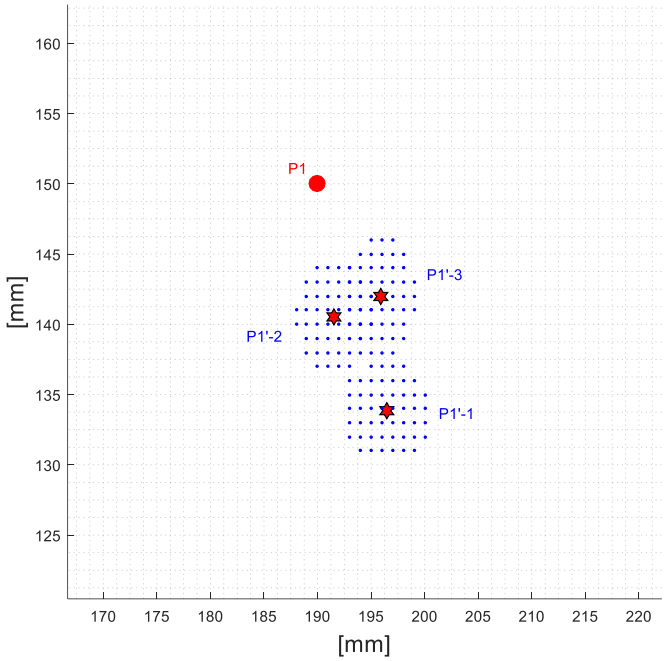

Figure 11. Zoom of results shown in Figures 8, 9 and 10. The illustration reports the real impact point P1 (red circle), the detected impact points P1′-1, P1′-2, P1′-3 (red stars) together with the points 1% above the minimum of the error function (blue dots). Reproduced from [24].

From Figures 8, 9, 10 and 11 we can observe that the accuracy of the localization of the impact coordinates is better using eight sensors respect to four sensors but the analysis with six sensors could be a good compromise between sensor density and the error obtained in impact localization. With the eight sensors analysis the localization error is of 2mm along the x-axis and 9 mm along the y-axis whereas processing signals acquired by six sensors the error is 6mm for the x-axis and 8 mm for the y-axis.

Figure 12 and Figure 13 demonstrate the ability of the electronic system to reveal also impacts outside the ROI with a good accuracy: for both cases, the error in the x-axis and y-axis impact point coordinates evaluation is less than 10mm.

Another observation is about the placement of sensors. In several real applications is not possible to install the sensors on the vertexes of regular geometric shapes (square, circle, hexagon, etc.) but the positions are decided by other constraints. From Figures 8-13 we can observe the position of the eight sensors that are symmetric along the x-axis (Rx1, Rx3, Rx4, Rx5, Rx7, Rx8) but non-symmetric along the y-axis (Rx2, Rx6): these results demonstrate that the calculated impact point is well identified even in case of non-symmetric positions of the sensors.

Preprints (www.preprints.org) | NOT PEER-REVIEWED | Posted: 22 April 2021 doi:10.20944/preprints202104.0595.v1

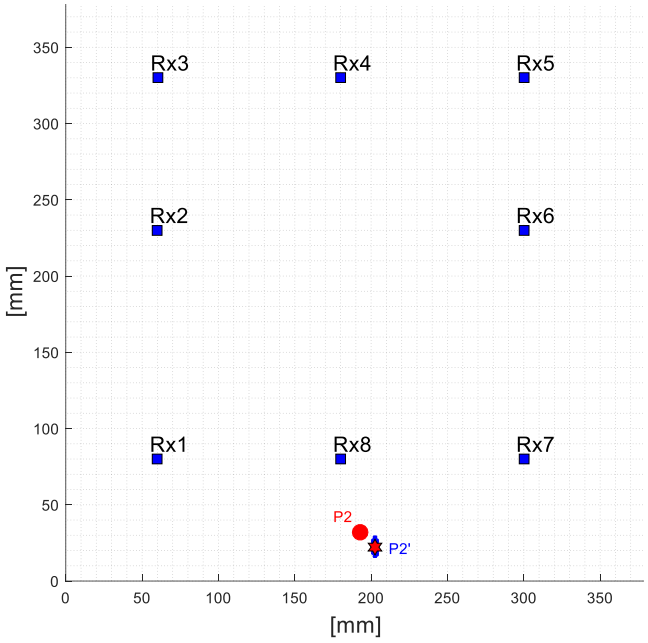

Figure 12. Position of impact P2 (red circle) outside the ROI. The detected impact position P2′ (red star) with coordinates xp = 202mm; yp = 22mm has been obtained by processing signals acquired by all sensors. Reproduced from [24].

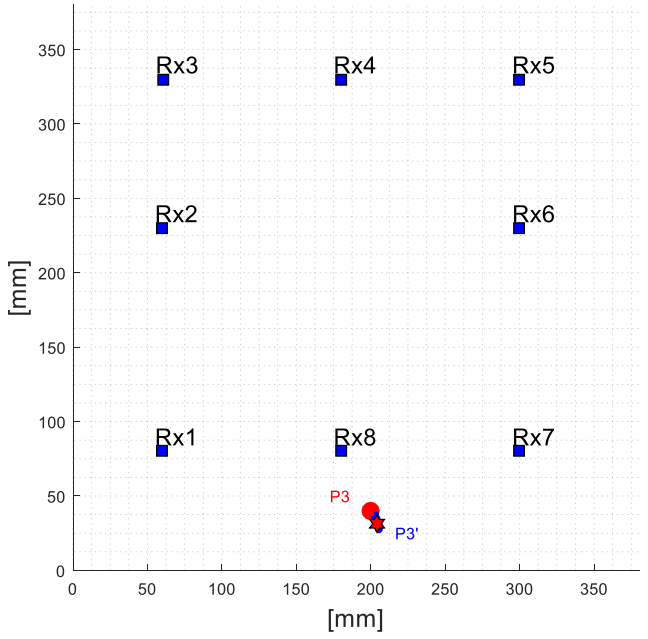

Figure 13. Position of impact P3 (red circle) outside the ROI. The detected impact position P3′ (red star) with coordinates xp = 205mm; yp = 32mm has been obtained by processing signals acquired by all eight sensors.

The resulting estimates of the three impacts P1, P2 and P3 are summarized in Table 2, Table 3, and Table 4, respectively. The errors of the impact localization are reported in % respect to the dimension of the monitored area that is 500 mm.

Preprints (www.preprints.org) | NOT PEER-REVIEWED | Posted: 22 April 2021 doi:10.20944/preprints202104.0595.v1

Table 2. Estimated impacts position obtained for impact P1' with coordinates xi = 190mm; yi = 150mm.

Predicted impact	Estimated position	Positioning error	Error=Positioning error/500mm %
P1'-1	x = 196mm	6mm (x-axis)	1.2%
	y = 134mm	16mm (y-axis)	3.2%
P1'-2	x = 192mm	2mm (x-axis)	0.4%
	y = 141mm	9mm (y-axis)	1.8%
P1'-3	x = 196mm	6mm (x-axis)	1.2%
	y = 142mm	8mm (y-axis)	1.6%

Table 3. Estimated impacts position obtained for impact P2' with coordinates xi = 193mm; yi = 32mm.

Predicted impact	Estimated position	Positioning error	Error =Positioning error/500mm %
P2'	x = 202mm	9mm (x-axis)	1.8%
	y = 22mm	10mm (y-axis)	2.0%

Table 4. Estimated impacts position obtained for impact P3' with coordinates xi = 200mm; yi = 40mm.

Predicted impact	Estimated position	Positioning error	Error %
P3'	x = 205mm	5mm (x-axis)	1.0%
	y = 32mm	8mm (y-axis)	1.6%

5. Discussion and final remarks.

This study presents the analysis of errors for impact location with different numbers of channels (from 4 to 8) connected to piezoelectric sensors on aluminum plate and front-end electronics capable to detect the early arrival signals of the S_0 mode. Impacts have been carried out inside and outside the defined ROI on the plate. To neglect the boundary reflections of the ultrasonic signal due to the free edges of the plate, an adhesive rubber has been used with the aim also to simulate a semi-infinite space outside the area delimited by the sensors. The DToA are obtained by the threshold method with real time electronics. The results of the experiments explain well the compromise between sensor density of a SHM system and error in impact location: the best accuracy is obtained with eight sensors covering an area of 500mm x 500mm in the aluminum laminate but a good compromise between sensor density and the error in impact localization has been detected processed the acquired signal by six sensors obtaining an error comparable with the assumed wavelength of the S_0 mode equal to 8mm. We found that the error is below 3.2% and slightly better for the x coordinate which is probably due to a systematic error on sensor reference coordinates. The main benefit of the AFE designed for this application is the possibility to select the best signal processing chain to avoid input saturation with large energy impact with sensors generating 1 to 10 Vpp amplitudes and retain high SNR better of 72 dB in the 270-800 kHz bandwidth. We also point out that a certain redundancy in the number of sensors is always useful to consider possible failures of single channels. Finally, thanks to the programmable configuration up to 16 channels, this criteria for the selection of the optimal sensor's density will be investigated also on CFRP plates with

same sensors layout for accounting the variability of velocity for composite laminates in different directions.

Author Contributions: "Conceptualization, E.M.M and L.C.; methodology, A.B.; software, E.M.M.; validation, E.:M.M and A.B.; formal analysis, E.M.M.; investigation, A.B. and L.C.; resources, L.C.; data curation, A.B.; writing—original draft preparation, L.C.; writing—review and editing, L.C.; visualization, E.M.M.; supervision, L.C.; project administration, L.C.; All authors have read and agreed to the published version of the manuscript.

Funding: This research received no external funding

Institutional Review Board Statement: Not applicable.

Informed Consent Statement: Not applicable.

Acknowledgments: The authors wish to acknowledge the support of this work of Mr. Marco Calzolai, senior technician at the Ultrasound and NDT laboratory of the University of Florence.

Conflicts of Interest: The authors declare no conflict of interest."

Appendix A

Acronym	
ADC	Analog to Digital Converter
AFE	Analog Front-End
AI	Artificial Intelligence
CFRP	Composite Fiber Reinforce Polymer
CWT	Continuous Wavelet Transform
DTOA	Differential Time of Arrival
IDT	Interdigital Transducer
NDT	Non-Destructive Testing
PVDF	Polyvinylidene fluoride
PZT	Lead zirconate titanate
ROI	Region Of Interest
SHM	Structural Health Monitoring
SNR	Signal to Noise Ratio
STFT	Short Time Fourier Transform

References

1. V. Giurgiutiu, "Structural Health Monitoring: With Piezoelectric Wafer Active Sensors", 2nd Edition. Elsevier, ISBN: 9780124186910, 24th June 2014, pages 1024
2. J.L. Rose, "Ultrasonic Guided Waves in Solid Media", Cambridge University Press: Cambridge, UK, 2014.
3. W. Ostachowicz, P. Kudela, M. Krawczuk, A. Zak, "Guided Waves in Structures for SHM: The Time-Domain Spectral Element Method", JohnWiley & Sons: New York, NY, USA, 2012. ISBN: 978-0-470-97983-9 February 2012, 350 Pages
4. A.S. Purekar, D.J. Pines, "Damage detection in thin composite laminates using piezoelectric phased sensor arrays and guided lamb wave interrogation", J. Intell. Mater. Syst. Struct. 2010, 21, pp. 995-1010.
5. L. Qiu, X. Deng, S. Yuan, Y. Huang, Y. Ren, "Impact monitoring for aircraft smart composite skins based on a lightweight sensor network and characteristic digital sequences", Sensors 2018, 18, pp. 2218.
6. A. Tobias, "Acoustic-emission source location in two dimensions by an array of three sensors", Non-Destr. Test, 1976, 9, 9-12.
7. F. Ciampa, M. Meo, "A new algorithm for acoustic emission localization and flexural group velocity determination in anisotropic structures", Compos. Part A Appl. Sci. Manuf. 2010, 41, pp. 1777–1786.
8. S. Mohd, K.M. Holford, R. Pullin, "Continuous wavelet transform analysis and modal location analysis acoustic emission source location for nuclear piping crack growth monitoring", In Proceedings of the AIP Conference Proceedings, Punjab, India, 17–21 December 2014; pp. 61–68.
9. S. Yin, Z. Cui, T. Kundu, "Acoustic source localization in anisotropic plates with "Z" shaped sensor clusters", Ultrasonics 2018, 84, pp. 34–37.

10. K. Worden, W.J. Staszewski, "Impact location and quantification on a composite panel using neural networks and a genetic algorithm", Strain 2000, 36, pp. 61–68.
11. S. Carrino, F. Nicassio and G. Scarselli, "An innovative method based on nonlinear Lamb waves for locating disbonds in Single-Lap joints," 2019 IEEE 5th International Workshop on Metrology for AeroSpace (MetroAeroSpace), Torino, Italy, 2019, pp. 187-191.
12. S. Carrino, F. Nicassio and G. Scarselli, " Non-linear Lamb Waves for Locating Defects in Single-Lap Joints" Frontiers in Built Environment Journal, Volume 6, Article 45, Aprile 2020.
13. T. Kundu "Acoustic source localization". Ultrasonics 2014, 54, pp 25-38.
14. N. Sen, T. Kundu, "A new wave front shape-based approach for acoustic source localization in an anisotropic plate without knowing its material properties", Ultrasonics, Vol. 87, pp. 20-32, 2018.
15. A. Bulletti, P. Giannelli, M. Calzolai, L. Capineri, "An Integrated Acousto/Ultrasonic Structural Health Monitoring System for Composite Pressure Vessels", IEEE Trans. Ultrason. Ferroelectr. Freq. Control 2016, 63, pp 864-873.
16. E. Marino Merlo, A. Bulletti, P. Giannelli, M. Calzolai, L. Capineri, "An Integrated Acousto/Ultrasonic Structural Health Monitoring System for Composite Pressure Vessels, A Novel Differential Time-of-Arrival Estimation Technique for Impact Localization on Carbon Fiber Laminate Sheets", Sensors 2017, 17, pp. 2270.
17. E. Marino Merlo, A. Bulletti, P. Giannelli, M. Calzolai, L. Capineri, "Analysis of Errors in the Estimation of Impact Positions in Plate-Like Structure through the Triangulation Formula by Piezoelectric Sensors Monitoring", Sensors 2018, 18, 3426.
18. M. Lehmann, A. Büter, B. Frankenstein, F. Schubert, B. Brunner, "Monitoring System for Delamination Detection - Qualification of Structural Health Monitoring (SHM) Systems", Conference on Damage in Composite Materials (CDCM), 2006.
19. K. Ono, «Review on Structural Health Evaluation with Acoustic Emission», Appl. Sci., vol. 8, n. 6, pp. 958, giu. 2018, doi: 10.3390/app8060958.
20. Q. Xinlin, L. Wenzhuo, W. Yishou, S. Hu, "Piezoelectric Transducer-Based Structural Health Monitoring for Aircraft Applications", Sensors 2019, 19(3).
21. L. Capineri, A. Bulletti, M. Calzolai, P. Giannelli, and D. Francesconi, "Arrays of conformable ultrasonic Lamb wave transducers for structural health monitoring with real-time electronics," Procedia Eng., vol. 87, pp. 1266-1269, 2014. doi: 10.1016/j.proeng.2014.11.408.
22. A. Ebrahimkhanlou, B. Dubuc, e S. Salamone, «A generalizable deep learning framework for localizing and characterizing acoustic emission sources in riveted metallic panels», Mech. Syst. Signal Process., vol. 130, pp. 248–272, set. 2019, doi: 10.1016/j.ymssp.2019.04.050.
23. R. Ross, «Structural health monitoring and impact detection using neural networks for damage characterization», in *47th AIAA/ASME/ASCE/AHS/ASC Structures, Structural Dynamics, and Materials Conference 14th AIAA/ASME/AHS Adaptive Structures Conference 7th*, 2006, pp. 2117.
24. A. Bulletti, E. M. Merlo and L. Capineri, "Analysis of the accuracy in impact localization using piezoe-lectric sensors for Structural Health Monitoring with multichannel real-time electronics," 2020 IEEE 7th International Workshop on Metrology for AeroSpace (MetroAeroSpace), Pisa, Italy, 2020.